ORIGINAL RESEARCH

Synthesis of pH stable, blue light-emitting diode-excited, fluorescent silica nanoparticles and effects on cell behavior

Shin-Woo Ha[1]
Jin-Kyu Lee[2]
George R Beck Jr[1,3,4]

[1]Division of Endocrinology, Department of Medicine, Emory University, Atlanta, GA, USA; [2]Department of Chemistry, Seoul National University, Seoul, South Korea; [3]The Atlanta Department of Veterans Affairs Medical Center, Decatur, [4]The Winship Cancer Institute, Emory University School of Medicine, Atlanta, GA, USA

Correspondence: George R Beck Jr
Division of Endocrinology, Department of Medicine, Emory University, 101 Woodruff Circle, 1026 WMRB, Atlanta, GA 30322, USA
Tel +1 404 727 1340
Fax +1 404 727 1300
Email george.beck@emory.edu

Shin-Woo Ha
Seoul National University Bundang Hospital, Healthcare Innovation Park, 3rd Floor, #W9, 172, Dolma-ro, Bundang-gu, Seongnam-si, Gyeonggi-do 13605, South Korea
Tel +82 31 787 8405
Fax +82 31 787 8709
Email shinwoo.ha@gmail.com

Abstract: To date, delivery of light-emitting diode (LED)-activated compounds to cells and tissue remains a challenge. Silica-based materials possess good biocompatibility and have advantages of control of size and shape. Fluorescent silica nanoparticles (NPs) have been synthesized and used for applications such as cell tracking and tumor identification. Here, we report the synthesis and optimization of fluorescent silica NPs, which incorporate a naphthalimide dye with triethoxysilanes that are excited by the blue LED wavelength (LEDex NPs). The NPs can be imaged in the 420–470 nm wavelength, demonstrate a high quantum yield, are stable in a range of pH, and are taken into the cells. Therefore, these NPs represent a novel imaging technology for biomedical applications.

Keywords: naphthalimide, imaging, bone marrow stromal cell migration, reduced toxicity

Introduction

Imaging is an important aspect of biomedical research widely used for cellular, molecular, and clinical applications as well as disease diagnosis providing a means to analyze tissues and cells nondestructively and with high precision. Laser microscopy such as confocal laser scanning microscopy (CLSM) is an important and commonly used technique in molecular biology to determine, for example, live or dead cells, to stain specific organelles such as endoplasmic reticulum and mitochondria, and to monitor intracellular pH. Various emission colors of the fluorescent agents are able to detect different events simultaneously. Furthermore, a state of the art laser microscope with super resolution can monitor on a scale of 100 nm. The light source is an important factor influencing the resolution of microscopy. In general, CLSM uses a laser as a light source for high resolution. Compared to other sources such as halogen and mercury lamps, a laser has a single line-like wavelength and it is very efficient for the excitation of fluorescent dyes. One disadvantage of this technology is that for the excitation of various dyes with different wavelengths, multiple lasers are required. Another is the result of the intense excitation energy in a concentrated area that can quickly photobleach many if not most fluorescent agents. Finally, the intense energy can also alter cells' properties such as generating reactive oxygen species[1] and damaging DNA, potentially leading to cell death by apoptosis.[2,3] Alternatives to high intensity laser for cellular imaging are therefore being investigated.

Light-emitting diode (LED) technology has been the focus of attempts to produce an eco-friendly, energy-efficient light source. The LEDs have various colors, ranging from UV (200–400 nm) to infrared region (>760 nm). Their full width half maximum

(FWHM) is narrow (20–70 nm), although similar to the extent of a laser, and they can be substituted in a laser microscope at a low cost (a few dollars) and require <1 cm of space. Among various colored LEDs, blue is considered a good candidate for imaging because the blue wavelength has a high energy and narrower FWHM, 20 nm less than other wavelengths. It has also been reported that a high-powered blue LED could be used for photo-bleaching experiments without the potentially negative consequences of heat that is often transferred from common light sources or the safety concerns of a high-powered laser.[4] In regard to toxicity, blue LED at 453 nm showed a less toxic profile up to 500 J/cm^2 compared to the shorter wavelength of violet-blue LED at 412–426 nm.[5] Therefore, LED technology may represent a significant advantage over current laser-based imaging agents for biomedical applications.

Silica nanoparticles (NPs) have many potential applications in biology and biomedicine because of important physical characteristics such as biocompatibility,[6,7] the ability to precisely control size and shape, color tunability, and photostability when combined with imaging agents.[8–10] Silicon dioxide (SiO$_2$) materials lack any emission property, and therefore, the excitation wavelength is dependent upon the incorporated dyes. Additionally, spherical silica NPs can be synthesized and size-controlled without any surfactants, and therefore, cell viability and/or associated toxicity by the surfactants is not a significant concern. Here, we report the design and synthesis of fluorescent silica NPs excited by blue LED wavelength (420–470 nm). The NPs excited by the blue LED (LEDex NPs) incorporate a naphthalimide (NI) dye with triethoxysilanes, which is capable of forming chemical bonding between the dye and silica matrix. Furthermore, we demonstrate that the synthesis of LEDex NPs can be controlled in the size range from 30 to 125 nm by the concentration of dyes, tetraethyl orthosilicate (TEOS) as a silica source, and ammonia. The resulting LEDex NPs show high quantum yield (QY) (~70%) and exhibit >40% of emission intensity for over a month in acidic to neutral pH. Finally, these NPs are biocompatible and are demonstrated to increase cell migration.

Materials and methods
Materials
TEOS was purchased from TCI (Tokyo, Japan), and the other chemicals were purchased from Sigma-Aldrich Co. (St Louis, MO, USA). All chemicals were used without further purification. The NI derivatives were characterized by ^{1}H and ^{13}C NMR (500 MHz; Varian, Palo Alto, CA, USA) and mass spectrometer (JMS-AX505WA; JEOL, Tokyo,

Japan). Photophysical properties were obtained by UV–visible spectrometer (S-3100; Scinco, Seoul, South Korea), fluorescence spectrophotometer (FP-6500; Jasco, Oklahoma City, OK, USA), and absolute QY system (C9920-02; Hamamatsu Photonics, Hamamatsu, Japan). Size and surface charge in different environments were measured by NanoComposix (San Diego, CA, USA).

### Synthesis of 2-allyl-6-bromo-1H-benzo[de]isoquinoline-1,3(2H)-dione, NI-1
The synthesis is generally summarized in Scheme 1A. A total of 1.4 g (5.1 mmol) of 4-bromo-1,8-naphthalic anhydride and 0.61 g (10.7 mmol) of allylamine were added in 50 mL of anhydrous ethanol.[11] After refluxing for 12 hours, it was cooled to room temperature and poured into 250 mL of water. A total of 1.56 g (98.7%) of yellow powder, NI-1, was taken by filtration, washed with water, and dried in vacuum with heat. ^{1}H NMR (500 MHz, DMSO-d$_6$); δ ppm 8.55 (q, 2H), 8.30 (d, 1H), 8.20 (d, 1H), 7.98 (t, 1H), 5.93 (m, 1H), 5.15 (dd, 2H), 4.64 (d, 2H) ^{13}C NMR (500 MHz, DMSO-d$_6$); δ ppm 163.28, 163.23, 133.42, 133.28, 132.37, 132.08, 131.75, 130.52, 129.95, 129.53, 129.04, 123.35, 122.58, 117.18, 42.58 HR-MS (CI+, M+1; C$_{15}$H$_{11}$BrNO$_2$); calculated (Calcd.) for 315.9973 m/z, observed (Obsd.) for 315.9971 m/z.

Synthesis of 2-allyl-6-(allylamino)-1H-benzo[de]isoquinoline-1,3(2H)-dione, NI-2
A total of 1 g (3.16 mmol) of NI-1, 3.63 g (36 mmol) of allylamine, and 0.3 g (1.2 mmol) of copper(II) sulfate pentahydrate were added in 45 mL of 2-methoxyethanol and refluxed.[12] After 3 hours, it was cooled to room temperature and poured into 250 mL of water. The precipitate was filtered, washed with water, and dried. A total of 0.525 g (57%) of yellow needle-shaped product was obtained by recrystallization with chlorobenzene. ^{1}H NMR (500 MHz, DMSO-d$_6$); δ ppm 8.71 (d, 1H), 8.44 (d, 1H), 8.24 (d, 1H), 8.10 (t, 1H), 7.70 (t, 1H), 6.71 (d, 1H), 5.96 (m, 2H), 5.25 (dd, 2H), 5.10 (dd, 2H), 4.62 (d, 2H), 4.07 (t, 2H) ^{13}C NMR (500 MHz, DMSO-d$_6$); δ ppm 164.13, 163.27, 151.27, 134.84, 134.82, 133.97, 131.45, 130.11, 129.29, 125.11, 122.50, 120.85, 116.80, 116.63, 108.43, 105.13, 45.61, 42.00 HR-MS (CI+, M+1; C$_{18}$H$_{17}$N$_2$O$_2$); Calcd. for 293.1290 m/z, Obsd. for 293.1281 m/z.

Synthesis of 2-(3-(trimethoxysilyl)propyl)-6-(3-(trimethoxysilyl)propylamino)-1H-benzo[de]isoquinoline-1,3(2H)-dione, NI-3
This reaction is similar to the previous report.[13] A total of 35 mg (0.12 mmol) of NI-2 was dissolved in 10 mL of

A

NI-1

NI-2

NI-3

B

TEOS

Hydrolysis–condensation
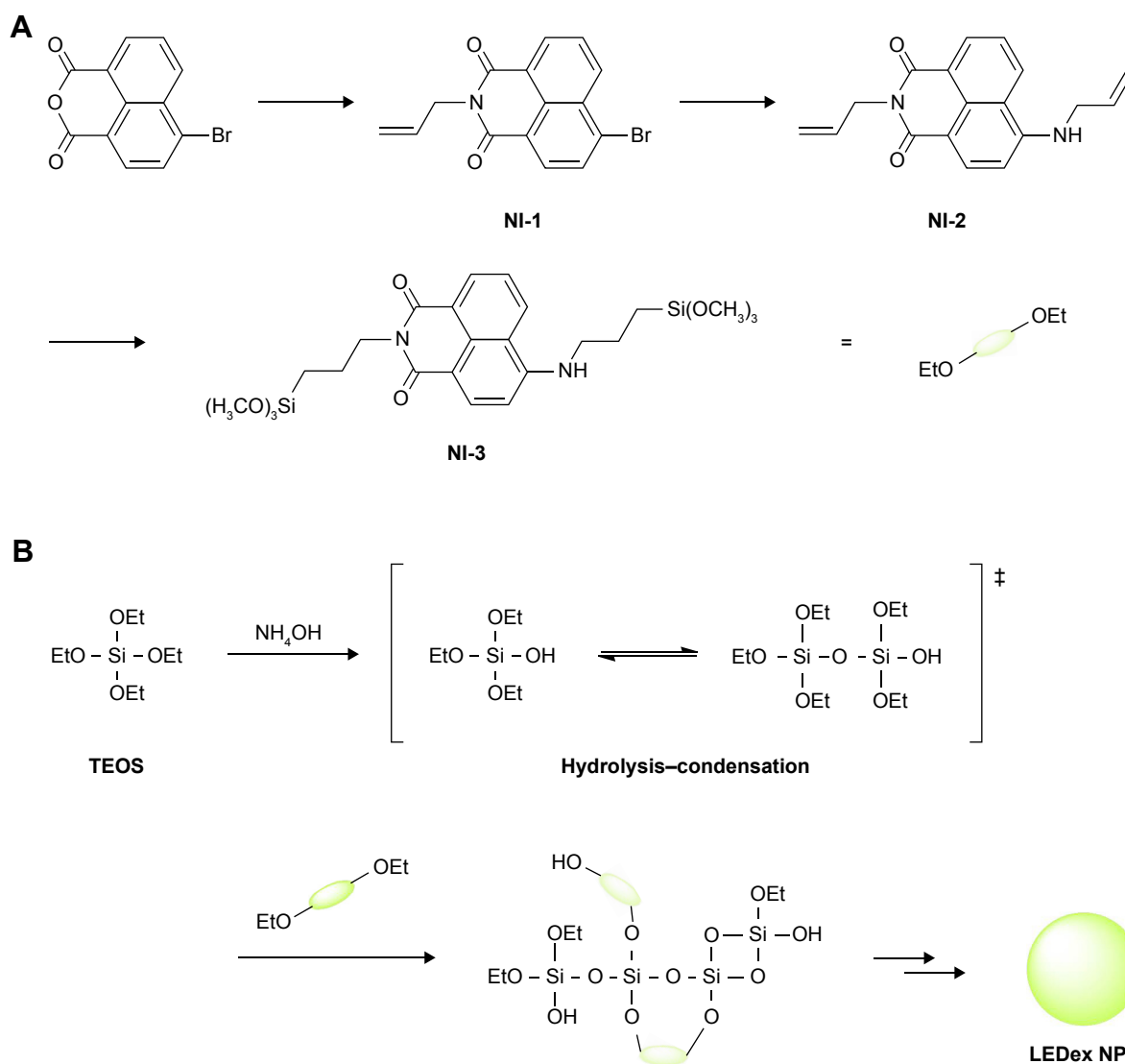
LEDex NPs

Scheme 1 Synthetic scheme of fluorescent dye (**A**) and silica NPs excited by blue LED (**B**).
Abbreviations: LED, light-emitting diode; NPs, nanoparticles; TEOS, tetraethyl orthosilicate; LEDex NPs, nanoparticles excited by the blue LED wavelength; Et; ethyl.

anhydrous chloroform. A total of 91 mg (0.1 mL, 0.75 mmol) of trimethoxysilane and a catalytic amount of Pt(dvs) in xylene were added, and the mixture was stirred at room temperature. After 6 hours, NI-3 was obtained by Celite filtration and vacuum dried at 60°C. ^{1}H NMR (500 MHz, CDCl$_3$); δ ppm 8.54 (q, 1H), 8.43 (d, 1H), 8.12 (dd, 1H), 7.58 (t, 1H), 6.68 (d, 1H), 4.13 (q, 2H), 3.58 (m, 18H), 3.4 (q, 2H), 1.85 (m, 4H), 1.09 (tt, 4H).

Synthesis of LEDex NPs and size control

The overall synthesis is generally summarized in Scheme 1B. TEOS 2.7 mL (12.1 mmol) was added in ethanol anhydrous with the as-prepared dye, NI-3, and stirred at 400 rpm for 5 min. Ammonia (14%) was added with stirring for 20 hours at room temperature. LEDex NPs were isolated by centrifugation; 18,000 rpm for 30 minutes for 30 nm and 15,000 rpm

for 20 minutes for the others. The supernatant was carefully decanted without disturbing the NP pellets, which were dispersed in ethanol by vortexing and sonication until all were clearly dispersed. This washing step was repeated five times. In the final step, the NP pellets were dispersed in the desired solutions such as alcohol, water, and PBS. The size and shape were characterized by transmission electron microscope (TEM; H7600; Hitachi Ltd., Tokyo, Japan). The size was controlled by varying the concentration of ammonia and dyes.

Surface modification of LEDex NPs

A total of 200 mg of the purified LEDex NPs were re-dispersed in 40 mL of ethanol anhydrous and then treated with 2-[methoxy(polyethyleneoxy)propyl] trimethoxysilane (mPEG-Si(OCH$_3$)$_3$: 1 g, fivefold excess by weight, PEO

repeating unit: 6–9, adjusting at pH 12 with ammonia. The PEGylated LEDex NPs were washed and centrifuged in ethanol three times followed by a single wash in sterile water.

Cell culture studies

Murine bone marrow stromal cells (BMSCs) were originally obtained from red marrow by centrifugation of the femur, as described in Camalier et al,[14] and frozen aliquots were used for the current studies and cultured for up to 20 passages. Cells were cultured in α-Modified Eagle's Medium (Thermo Fisher Scientific, Waltham, MA, USA) supplemented with 10% fetal bovine serum (FBS; Atlanta Biologicals, Lawrenceville, GA, USA) supplemented with 1% L-glutamine (Thermo Fisher Scientific) and 1% of penicillin/streptomycin (Thermo Fisher Scientific).[15] All cell lines were cultured at 37°C in 5% CO_2. Cell viability was measured using a commercial 3-(4,5-dimethylthiazol-2-yl)-5-(3-carboxyl-methoxyphenyl)-2-(4-sulfonyl)-2H-tetrazolium (XTT) assay according to the manufacturer's protocol (Promega Corporation, Fitchburg, WI, USA) as described previously.[6] Cells were plated at ~5×10^3 cells/well (~50%–60% confluent) in 96-well plates. After 24 hours, NPs were added as indicated, and 3 days later, the cells were analyzed using XTT (20 µL in 100 µL) assay reagent on a spectrophotometer (SpectraMAX250; Molecular Devices LLC, Sunnyvale, CA, USA). Scratch wound assays were performed on cells that had reached 95% density. Percent area is (newly covered area after 24 hours/total initial uncovered area) ×100. Percent width is ([newly covered area after 24 hours/total initial uncovered area]/length) ×100. Simply, area = $L \times W$ and width = area/L. Confocal microscopy was performed on BMSCs incubated with LEDex NPs for 24 hours. Images were captured by Zeiss (Oberkochen, Germany) LSM 510 META point scanning laser confocal microscope.

Results and discussion

Control of nanomaterial size and shape is crucial because these properties have been demonstrated to influence the interface with the biology. For example, 50 nm gold spherical NPs are internalized by cells more rapidly than gold NPs of other sizes and shapes,[16] which may be the result of different cellular mechanisms of internalization.[17] Size and shape also present different in vitro toxic profiles[18,19] and different organ distributions.[20] To control the shape or size of silica nanomaterials, the concentration of TEOS, ammonia, and surfactants is varied.[13,21] The rod-like shape can be controlled by a surfactant, which directly affects cell viability and can also control porosity.[22,23] As such, the excess surfactants have

to be removed for biological applications, or reduced cell viability will occur.[24] The emission color can be easily tuned by incorporating organic dyes,[13] inorganic complexes,[25] dye ratios,[26] or quantum dots.[27] Their excitation is necessary for emission to observe cell or organelle location or track changes in cell behavior. UV excites various dyes and is therefore a broadly utilized light source. However, its intrinsically high energy can damage cells, such as a UV lamp in the biological safety cabinet, which is used for sterilization or cause photobleaching as a result of decreased fluorescence from dyes. To minimize biological damage and photobleaching, we chose an NI dye to enable use of a lower energy source than UV and incorporation into spherical 50 nm silica NPs for photostability.

The NI dye was synthesized based on previous reports.[11,12] The first step is the addition of amine into anhydride (Scheme 1A). Weak fluorescence of NI-1 could be only detected by a spectrophotometer. After substituting a halogen group at the 4 position, bright fluorescence was detected under UV light because of internal charge transfer transition. The introduction of functional groups for designed applications and photophysical properties are controllable.[28] Finally, hydrosilylation was conducted under platinum catalyst with quantitative yield (Scheme 1B).[13] The dye was obtained with an overall high yield of 56%. The hydrosilylated, NI-3 has six reactive methoxysilane groups. For characterization of photophysical properties, NI-2 was used. The NI dye showed high QY, large stokes shift (~100 nm), and high extinction coefficient; 90% excited at 423 nm and 78% at 470 nm in chloroform (Figure S1). In ethanol, 69% of QY was recorded at 470 nm (Figure S2). The extinction coefficient represents the extent of light absorbance of a molecule and was measured to 8.8×10^3/M/cm in chloroform and 1.6×10^4/M/cm in ethanol (Figure S3).

The LEDex NPs were synthesized with dyes, TEOS, and ammonia in ethanol (solvent) to generate a spherical shape and without surfactants to reduce or eliminate any potential cell toxicity. TEOS and dyes were chemically linked by hydrolysis and condensation. Excess chemicals were completely removed by a multiple washing process until the fluorescence in washing solution was not detected by spectrophotometer and its pH reached nearly neutral as determined by a pH meter. The size of the NPs is mainly regulated by the concentration of TEOS and ammonia. We tested this by first keeping TEOS at constant, while varying the concentration of ammonia. The NPs were successfully controlled in the size range from 30 to 120 nm. Ammonia acts as a basic catalyst to accelerate hydrolysis–condensation reaction and

Table 1 Reaction condition and size of fluorescent LEDex nanoparticles

Entry	Reaction condition				Results, size (nm)
	Dye (mM)	TEOS (mM)	14% NH₄OH (mL)	Ethanol (mL)	
1	1.0	96.7	10	112	26.8±2.7
2	0.5	96.7	8	114	29.9±4.1
3	0.2	96.7	8	114	46.6±6.0
4	0.1	96.7	8	114	84.3±6.0
5	0.2	96.7	12	110	109.1±10.7
6	0.2	96.7	16	106	116.1±10.6

Notes: The reactions were performed at room temperature and constantly stirred at 400 rpm during the reaction. A total of 14% ammonia solution (NH_4OH) was half diluted with deionized water from 28% solution before the addition. Ethanol was used as a solvent and to adjust total reaction volume. The size was measured in water.
Abbreviations: LED, light-emitting diode; TEOS, tetraethyl orthosilicate; LEDex NPs, nanoparticles excited by the blue LED wavelength.

directly affects size.[13,29] To confirm the relationship between ammonia concentration and size, we varied the concentration of 14% ammonia from 8 to 16 mL under the same concentration of dye. For every 0.2 mM (14 mg) of the dye, the size is increased from 50 to 120 nm (#3, #5, and #6 in Table 1). Furthermore, higher concentrations of ammonia resulted in larger sized particles.[30] Compared to the NPs generated from 8 mL ammonia-added NPs, the 12 mL ammonia-added NPs were 60 nm larger in size (#3 vs #5 in Table 1). However, with 16 mL ammonia-added NPs, the NPs only increased by 15 nm in size, which was likely due to the limitation of available TEOS.

To determine if the dye concentration affected the size, we varied the dye concentration while the other components were kept constant. Increasing the dye concentration, resulted in decreased size, from 90 to 30 nm, the opposite effect of ammonia (#1 to #4 in Table 1). Considering that methoxysilane is more reactive than ethoxysilane in hydrolysis–condensation,[31] it was thought that the dye acts as a seed because our dye has two trimethoxysilane groups. We also hypothesized that if the growth rate is independent of size, the higher concentration of dye can spontaneously generate more seeds, from which NPs were continuously initiated until all component sources were depleted. A lower concentration of dye generates fewer seeds, and therefore, the particles had more available resources to increase in size and the low dye concentration generated larger NPs while at the high dye concentration the NPs were smaller. The as-prepared NP weight was slightly greater than the ideal calculation (100%). Assuming that this is 1:1 reaction because oxygen can be taken from TEOS and water and that for the calculated TEOS (molecular weight [Mw] 208.33 g/mol) conversion to SiO_2 (Mw 60.08 g/mol), all TEOS is consumed to generate

NPs; the calculated result was 0.73 g of NPs. In practice, 0.76–0.88 g was obtained from all samples after final purification. The practical was heavier than the calculation because it is possible that the NPs have numerous Si–OH groups, not fully condensed to Si–O in- and outside. This is supported by our previous report that the as-prepared silica NPs have numerous Si–OH groups (on the surface and in the NP) as determined by ²⁹Si CP-MAS NMR, in which spectra Q3 silicon atoms having one OH group and three oxygen bridges showed higher intensity or wider area of peaks than Q4 silicon atoms with all oxygen bridges. Even though some of Q3 peaks were transformed to Q4 by the aging process and what remained were a majority of Q3 peaks.[32]

Synthesized LEDex NPs (OH terminated) are well dispersed in acetone, alcoholic solvent, water, and biological media without any surface modifications (Figure 1). The NI dye is not soluble in water, and therefore, it is difficult to investigate if the fluorescent property of the dye is solvent-dependent. After incorporation of the dye into the silica, the solubility is independent of solvents and the dye-incorporated silica NPs should be soluble in polar organic solvents such as acetone and ethanol. We tested three solvents, acetone, ethanol, and water. All three concentrations are matched by UV–visible absorption intensity and are excited at 470 nm. Fluorescent intensity in acetone and ethanol were similar; however, in water, it was remarkably decreased (Figure 1). Even though the silica matrix encloses the dyes and helps to change their solubility, the silica cannot perfectly protect the contact between the dyes and solvent molecules, leading to a decrease in the fluorescent intensity in water.

NPs used for drug delivery or biological imaging have to be tolerated and not to lose their unique or enhanced properties in the harsh physiological pH. Addition of polyethyleneglycol (PEG or PEGylation) is one of the most important surface modifications for biological/biomedical applications; PEGylation not only increases the stability of NPs in biological media such as PBS and culture media but also, for in vivo applications, enhances their circulation time against the reticulo-endothelial system, the mechanism by which many NPs are removed from the circulation, accumulating in liver or spleen.[33] Therefore, PEGylation can increase the efficiency of passive targeting. PEGylation was performed by the introduction of mPEG-Si(OMe)₃ molecule on the surface. The trimethoxysilane group in the molecule is chemically bounded by hydrolysis–condensation. Zeta potentials were not dramatically changed between before (−45.8±1.2 mV) and after PEGylation (−43.1±0.9 mV) because many OH groups inside the NPs still remain.
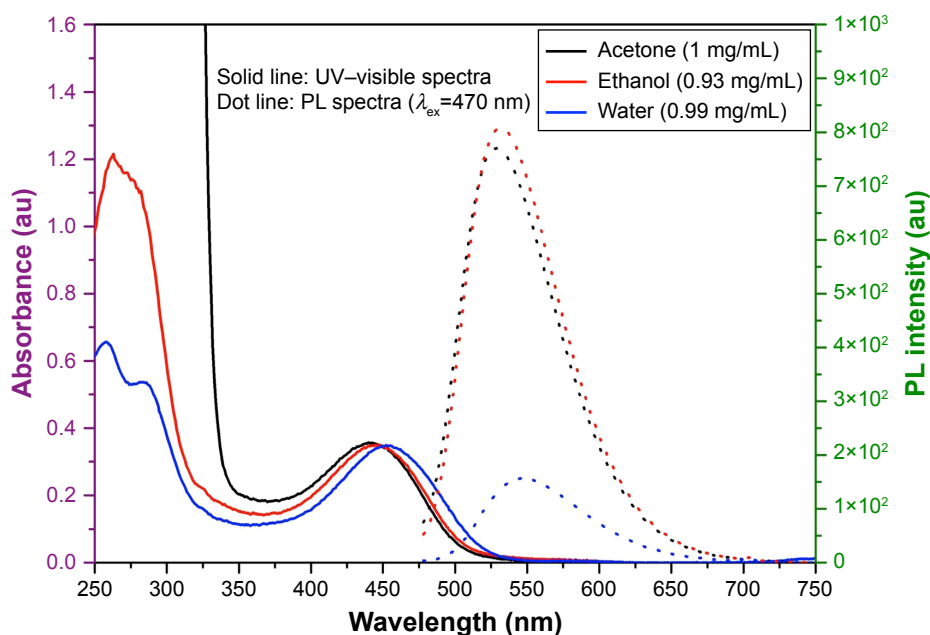
Figure 1 Absorption and emission spectra of LEDex nanoparticles in acetone, ethanol, and water.
Note: LEDex nanoparticles were dispersed in solvent as indicated and measured for absorbance and PL (it is similar to fluorescent) intensity by UV–visible spectrometer and fluorescent spectrophotometer.
Abbreviations: LED, light-emitting diode; PL, photoluminescent; LEDex NPs, nanoparticles excited by the blue LED wavelength.

Biomedical applications are more likely to expose NPs to an acidic rather than a basic environment; in cells, the pH can vary from ~5.5 to 6.5 in the endosome to ~4.5 in the lysosome.[34] Physiologic pH in the human body ranges from ~3 in the stomach to ~5–6 in the small intestine and 7 in the colon.[35] We therefore tested the pH stability of our NPs by adjusting the pH to 3, 5, and 7 with hydrochloric acid. The PEGylated particles did not change in size regardless of pH; however, the OH terminated did increase from 77 to 110 nm (Figure 2A). Interestingly, the zeta potential did not change significantly as the pH dropped to 3, (Figure 2B). Collectively, the results

suggest that the surface was successfully modified and, therefore, the PEGylated size was not affected by pH compared to the OH whereas the zeta potential might reflect the overall charge of NPs not the surface charge.

To test the long-term stability under the varying pHs, both LEDex NPs (OH-terminated and PEGylated) were exposed to pH (3–7) and monitored for >1 month by spectrophotometer for emission property and TEM for morphological change. The concentrations of the NPs were identically matched to 1 mg/mL in water. After 31 days in the varying pHs, no change in morphology or obvious aggregation was observed
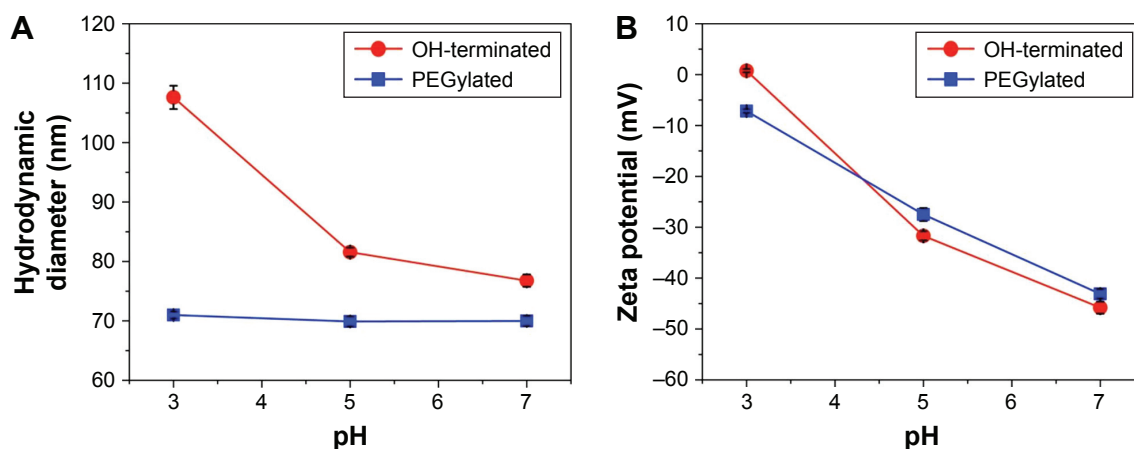

Figure 2 Size and surface charge of the LEDex nanoparticles in varying pH.
Notes: LEDex nanoparticles (OH-terminated and PEGylated) were dispersed in water (3–7; adjusted with HCl) for three times and hydrodynamic diameter (nm) (**A**) and zeta potential (mV) (**B**) measured by zeta sizer.
Abbreviations: LED, light-emitting diode; LEDex NPs, nanoparticles excited by the blue LED wavelength; HCl, hydrogen chloride.
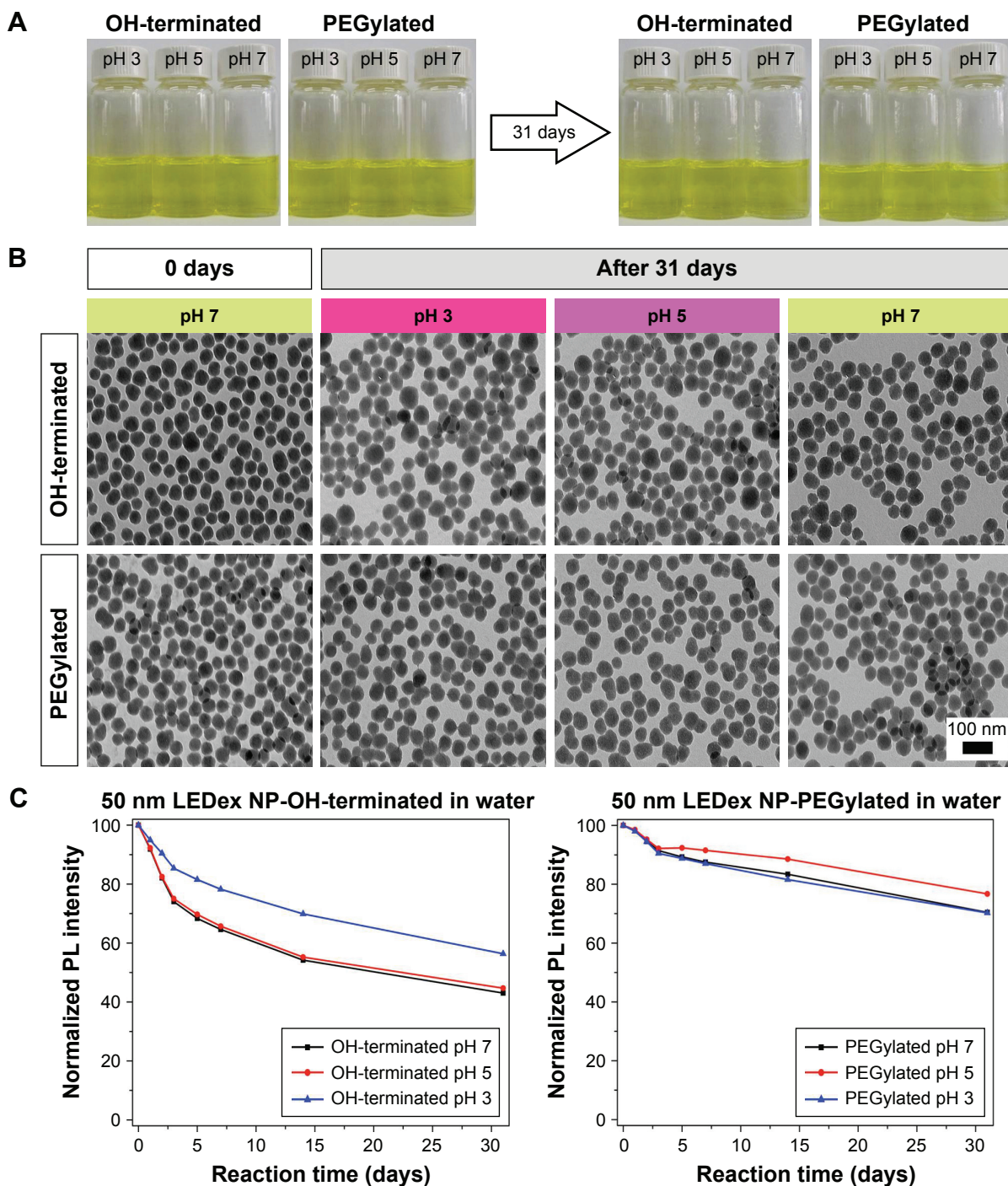
Figure 3 TEM characterization and fluorescent intensity of OH-terminated and PEGylated LEDex NPs in varying pH for 31 days.
Notes: (**A**) LEDex NPs (OH-terminated and PEGylated) were incubated in water at varying pH (3–7; adjusted with HCl) for 31 days, and stability and dispersibility of LEDex nanoparticles were visualized followed by (**B**) imaging with TEM. (**C**) Fluorescent intensity of LEDex nanoparticles (OH-terminated and PEGylated) (1 mg/mL) in varying pH (3–7; adjusted with HCl) was measured by photoluminescence over time as indicated.
Abbreviations: LED, light-emitting diode; NP, nanoparticle; LEDex NPs, nanoparticles excited by the blue LED wavelength; PL, photoluminescent; TEM, transmission electron microscope; HCl, hydrogen chloride.

by TEM (Figure 3A and B). Fluorescent intensity was also time-dependently recorded. All measurement parameters were nearly identical over time. The OH terminated lost 40% of fluorescence after the first week and an additional 10% over the next 3 weeks (Figure 3C) while the PEGylated LEDex NPs lost only an average of 12% and an additional 16% over the same times. In total, the OH lost >50% and the PEGylated lost <30% over the 31 days (Figure 3C). Therefore, the PEG surface modification is very helpful for maintaining photophysical properties in different physiological pHs.
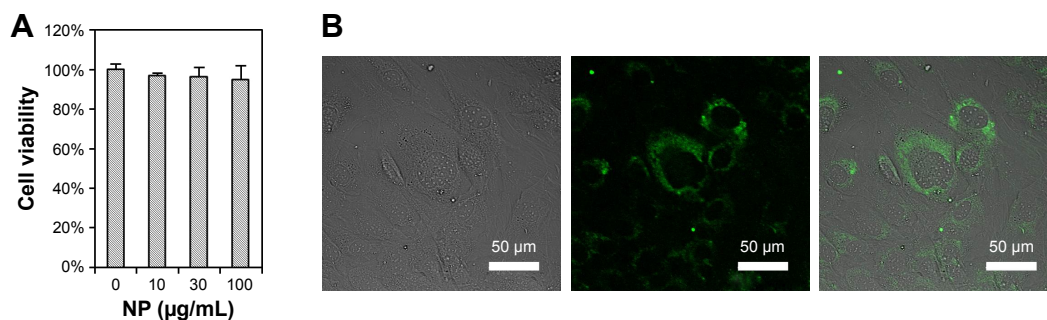
Figure 4 Confocal laser scanning microscopy images of PEGylated LEDex NPs.
Notes: (**A**) Cell viability was measured in BMSCs after 3 days of treatment with LED NPs at concentrations as indicated. (**B**) BMSCs were incubated with LEDex NPs (30 µg/mL) for 24 hours and imaged; excited by 488 nm laser and monitored with FITC filter set, scale bar is 50 µm.
Abbreviations: BMSCs, bone marrow stromal cells; LED, light-emitting diode; NPs, nanoparticles; LEDex NPs, nanoparticles excited by the blue LED wavelength.

Most bio-imaging applications require that the imaging agent be compatible with cell viability. To determine if the LEDex NPs were compatible with cells in culture, a cell viability assay was performed using aliquots of murine BMSCs originally isolated from red marrow by centrifugation of the femur.[14] BMSCs generally represent cells of the adherent mesenchyme lineage. BMSCs were treated with increasing concentrations of LEDex NPs. Results demonstrated that the LEDex NPs were nontoxic for up to 3 days at concentration up to 100 µg/mL (Figure 4A). To determine if our NPs can be observed by blue excitation, we added PEGylated LEDex NPs to the medium of BMSCs for 24 hours. Using CLSM, the LEDex NPs could be clearly observed by fluorescent microscopy (Figure 4B). The NPs are located in cytoplasm but not in the nucleus in agreement with previous studies using red-fluorescent 50 nm silica-based NPs.[6,13,36] Spherical 50 nm silica NPs have been demonstrated to be internalized by most cell types and from varying origins,[6] and it is therefore expected that LEDex NPs will also act in a similar manner. Taken together, the results demonstrate that these LEDex NPs can be used as a novel cell imaging agent.

Our imaging studies appeared to show that the cells were more active on the cell culture plates. To test the hypothesis that the LEDex NPs triggered cell movement and migration, we conducted a scratch assay. BMSCs were plated in a six-well plate. Once the cells reached 95% density, cross-lines were scratched (Figure 5A). The NPs were then added to cells grown in either growth medium (Figure 5B) or serum-free medium (Figure 5C) for 24 hours. The cells were photographed by brightfield microscopy and the images analyzed for quantification using Adobe Photoshop CC (Adobe systems, San Jose, CA, USA) and ImageJ (NIH, Rockville, MD, USA). Results revealed that NP-treated cells under both growth and serum-free medium conditions were >10% enhanced for migration (Figure 5D and E).

To date, there are limited data on the effects of silica NPs on migration. One study, using 59 nm spherical amorphous silica NPs, found inhibition of cell migration in the absence of FBS,[37] whereas another study using 100 nm spherical mesoporous NPs in the presence of FBS found an increase in cell migration.[38] Both studies suggest rearrangement of cytoskeletal structures, and this is possible with LEDex NPs because of its cellular uptake (Figure 4). Therefore, one mechanism may involve NPs triggering intracellular events, which alter the cytoskeleton and drive changes in cell behavior. A second mechanism might involve altered topography. Surface topography can also have a significant influence on behavior related to attachment with increasing roughness increasing adhesion and proliferation.[39] It is therefore possible that the NPs bind the plate surface thereby increasing surface roughness and cell migration. It should be noted that these two potential mechanisms are not mutually exclusive.

Conclusion

Here, we have reported the synthesis and characterization of fluorescent NPs excited by commercial blue LED. The use of LEDex NPs for biomedical imaging provides a number of advantages over more traditional laser excited imaging methods including a smaller equipment footprint and cost, but more importantly they represent an additional method to image cells without the high energy required by a laser. The ability to use lower energy thereby reduces potential toxicity from hyperthermia and other off-target effects such as increased reactive oxygen species. Recent studies have demonstrated the potential use of LED light sources for biomedical applications. Blue wavelength LEDs have been used in medical applications such as polymerization of dental composites and treatment of rheumatoid arthritis, whereas red wavelength LEDs have been applied to wound healing and acne treatment.[40] The use of blue wavelength
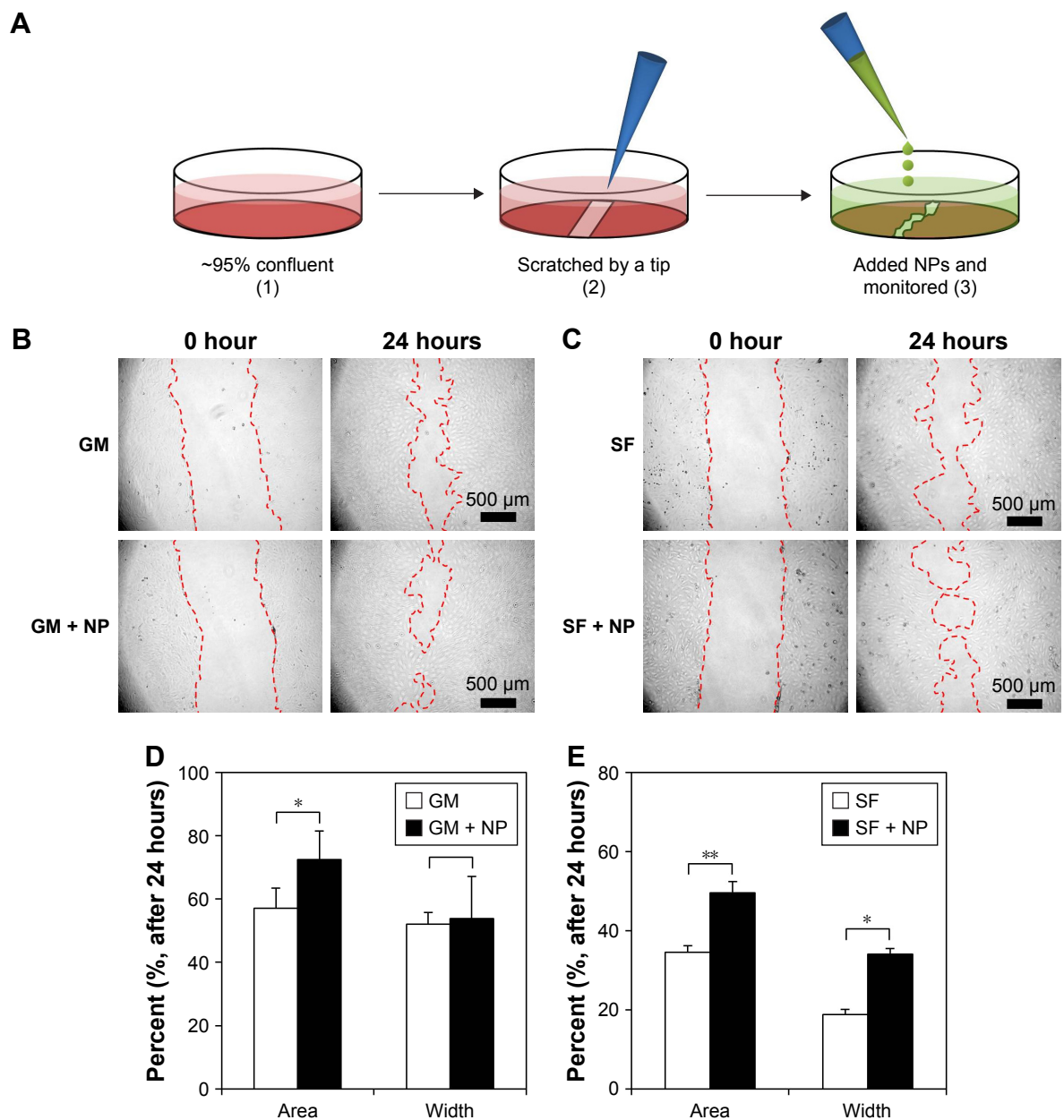
A

~95% confluent
(1)

Scratched by a tip
(2)

Added NPs and
monitored (3)

B

C

D

E

Figure 5 Cell migration effects of PEGylated LEDex NPs.
Notes: (**A**) Schematic representation of scratch wound assay with LEDex NPs. (**B**) BMSCs were cultures in (**A**) GM or (**C**) SF media for 24 hours and cell migration measured in a scratch wound assay. (**D**) Quantification analysis of (**B**). (**E**) Quantification analysis of (**C**). Scale bar is 500 µm. Quantification of covered area and covered width was performed using Adobe Photoshop CC (Adobe systems, San Jose, CA, USA) and ImageJ analyses (NIH, Rockville, MD, USA). Three images were analyzed and averaged. $*P<0.05$ and $**P<0.005$ relative to non-NP treated, by Student's t-test.
Abbreviations: BMSCs, bone marrow stromal cells; GM, growth media; LED, light-emitting diode; NPs, nanoparticles; LEDex NPs, nanoparticles excited by the blue LED wavelength; SF, serum free.

LED has been applied to microscopy to successfully image hippocampal astrocytes labeled with antibodies against the astrocytic marker GFAP.[41] Taken together, results reported herein demonstrate the synthesis of a novel cell compatible blue LEDex NPs using NI dye, which is pH stable and demonstrates a high QY and, therefore, represents a novel reagent for biomedical imaging.

Acknowledgments

the Department of Veterans Affairs, National Institutes of Health, or the United States Government.

Disclosure
The authors report no conflicts of interest in this work.

References
1. Heck DE, Vetrano AM, Mariano TM, Laskin JD. UVB light stimulates production of reactive oxygen species: unexpected role for catalase. *J Biol Chem*. 2003;278(25):22432–22436.
2. Rastogi RP, Richa Kumar A, Tyagi MB, Sinha RP. Molecular mechanisms of ultraviolet radiation-induced DNA damage and repair. *J Nucleic Acids*. 2010;2010:592980.
3. Song J, Gao T, Ye M, Bi H, Liu G. The photocytotoxicity of different lights on mammalian cells in interior lighting system. *J Photochem Photobiol B*. 2012;117:13–18.
4. Herman TK, Mackowiak SA, Kaufman LJ. High power light emitting diode based setup for photobleaching fluorescent impurities. *Rev Sci Instrum*. 2009;80(1):016107.
5. Liebmann J, Born M, Kolb-Bachofen V. Blue-light irradiation regulates proliferation and differentiation in human skin cells. *J Invest Dermatol*. 2010;130(1):259–269.
6. Ha SW, Sikorski JA, Weitzmann MN, Beck GR Jr. Bio-active engineered 50 nm silica nanoparticles with bone anabolic activity: therapeutic index, effective concentration, and cytotoxicity profile in vitro. *Toxicol In Vitro*. 2014;28(3):354–364.
7. Liberman A, Mendez N, Trogler WC, Kummel AC. Synthesis and surface functionalization of silica nanoparticles for nanomedicine. *Surf Sci Rep*. 2014;69(2–3):132–158.
8. Bae SW, Tan WH, Hong JI. Fluorescent dye-doped silica nanoparticles: new tools for bioapplications. *Chem Commun*. 2012;48(17):2270–2282.
9. Wolfbeis OS. An overview of nanoparticles commonly used in fluorescent bioimaging. *Chem Soc Rev*. 2015;44(14):4743–4768.
10. Kang Z, Liu Y, Lee ST. Small-sized silicon nanoparticles: new nanolights and nanocatalysts. *Nanoscale*. 2011;3(3):777–791.
11. Konstantinova TN, Meallier P, Grabchev I. The synthesis of some 1,8-naphthalic anhydride derivatives as dyes for polymeric materials. *Dyes Pigm*. 1993;22(3):191–198.
12. Grabtchev I, Konstantinov T, Guittonneau S, Meallier P. Photochemistry of some 1,8-naphthalic anhydride derivatives. *Dyes Pigm*. 1997;35(4):361–366.
13. Ha SW, Camalier CE, Beck GR Jr, Lee J-K. New method to prepare very stable and biocompatible fluorescent silica nanoparticles. *Chem Commun (Camb)*. 2009;(20):2881–2883.
14. Camalier CE, Yi M, Yu LR, et al. An integrated understanding of the physiological response to elevated extracellular phosphate. *J Cell Physiol*. 2013;228(7):1536–1550.
15. Beck GR Jr, Ha SW, Camalier CE, et al. Bioactive silica-based nanoparticles stimulate bone-forming osteoblasts, suppress bone-resorbing osteoclasts, and enhance bone mineral density in vivo. *Nanomedicine*. 2012;8(6):793–803.
16. Chithrani BD, Ghazani AA, Chan WC. Determining the size and shape dependence of gold nanoparticle uptake into mammalian cells. *Nano Lett*. 2006;6(4):662–668.
17. Petros RA, DeSimone JM. Strategies in the design of nanoparticles for therapeutic applications. *Nat Rev Drug Discov*. 2010;9(8):615–627.
18. Napierska D, Thomassen LC, Rabolli V, et al. Size-dependent cytotoxicity of monodisperse silica nanoparticles in human endothelial cells. *Small*. 2009;5(7):846–853.
19. Sohaebuddin SK, Thevenot PT, Baker D, Eaton JW, Tang LP. Nanomaterial cytotoxicity is composition, size, and cell type dependent. *Part Fibre Toxicol*. 2010;7:22.

20. De Jong WH, Hagens WI, Krystek P, Burger MC, Sips AJAM, Geertsma RE. Particle size-dependent organ distribution of gold nanoparticles after intravenous administration. *Biomaterials*. 2008;29(12):1912–1919.
21. Huang XL, Li LL, Liu TL, et al. The shape effect of mesoporous silica nanoparticles on biodistribution, clearance, and biocompatibility in vivo. *ACS Nano*. 2011;5(7):5390–5399.
22. Huh S, Wiench JW, Yoo JC, Pruski M, Lin VSY. Organic functionalization and morphology control of mesoporous silicas via a co-condensation synthesis method. *Chem Mater*. 2003;15(22):4247–4256.
23. Wu SH, Mou CY, Lin HP. Synthesis of mesoporous silica nanoparticles. *Chem Soc Rev*. 2013;42(9):3862–3875.
24. Connor EE, Mwamuka J, Gole A, Murphy CJ, Wyatt MD. Gold nanoparticles are taken up by human cells but do not cause acute cytotoxicity. *Small*. 2005;1(3):325–327.
25. Kim OH, Ha SW, Il Kim J, Lee JK. Excellent photostability of phosphorescent nanoparticles and their application as a color converter in light emitting diodes. *ACS Nano*. 2010;4(6):3397–3405.
26. Wang L, Tan WH. Multicolor FRET silica nanoparticles by single wavelength excitation. *Nano Lett*. 2006;6(1):84–88.
27. Gerion D, Pinaud F, Williams SC, et al. Synthesis and properties of biocompatible water-soluble silica-coated CdSe/ZnS semiconductor quantum dots. *J Phys Chem B*. 2001;105(37):8861–8871.
28. Banerjee S, Veale EB, Phelan CM, et al. Recent advances in the development of 1,8-naphthalimide based DNA targeting binders, anti-cancer and fluorescent cellular imaging agents. *Chem Soc Rev*. 2013;42(4):1601–1618.
29. Cushing BL, Kolesnichenko VL, O'Connor CJ. Recent advances in the liquid-phase syntheses of inorganic nanoparticles. *Chem Rev*. 2004;104(9):3893–3946.
30. Stober W, Fink A, Bohn E. Controlled growth of monodisperse silica spheres in the micron size range. *J Colloid Interface Sci*. 1968;26(1):62–69.
31. Hermanson GT. Introduction to bioconjugation. *Bioconjugate Techniques*. 3rd ed. San Diego: Academic Press. 2013:1–125.
32. Lee WM, Ha SW, Yang CY, Lee JK, An YJ. Effect of fluorescent silica nanoparticles in embryo and larva of *Oryzias latipes*: sonic effect in nanoparticle dispersion. *Chemosphere*. 2011;82(3):451–459.
33. Jokerst JV, Lobovkina T, Zare RN, Gambhir SS. Nanoparticle PEGylation for imaging and therapy. *Nanomedicine*. 2011;6(4):715–728.
34. Gilleron J, Querbes W, Zeigerer A, et al. Image-based analysis of lipid nanoparticle-mediated siRNA delivery, intracellular trafficking and endosomal escape. *Nat Biotechnol*. 2013;31(7):638–646.
35. Laroui H, Wilson DS, Dalmasso G, et al. Nanomedicine in GI. *Am J Physiol Gastrointest Liver Physiol*. 2011;300(3):G371–G383.
36. Ha SW, Camalier CE, Weitzmann MN, Beck GR, Lee J-K. Long-term monitoring of the physicochemical properties of silica-based nanoparticles on the rate of endocytosis and exocytosis and consequences of cell division. *Soft Mater*. 2013;11(2):195–203.
37. Gonzalez L, De Santis Puzzonia M, Ricci R, et al. Amorphous silica nanoparticles alter microtubule dynamics and cell migration. *Nanotoxicology*. 2015;9(6):729–736.
38. Huang X, Teng X, Chen D, Tang F, He J. The effect of the shape of mesoporous silica nanoparticles on cellular uptake and cell function. *Biomaterials*. 2010;31(3):438–448.
39. San Miguel B, Kriauciunas R, Tosatti S, et al. Enhanced osteoblastic activity and bone regeneration using surface-modified porous bioactive glass scaffolds. *J Biomed Mater Res A*. 2010;94(4):1023–1033.
40. Yeh NG, Wu CH, Cheng TC. Light-emitting diodes-Their potential in biomedical applications. *Renew Sustain Energy Rev*. 2010;14(8):2161–2166.
41. Albeanu DF, Soucy E, Sato TF, Meister M, Murthy VN. LED arrays as cost effective and efficient light sources for widefield microscopy. *PLoS One*. 2008;3(5):e2146.
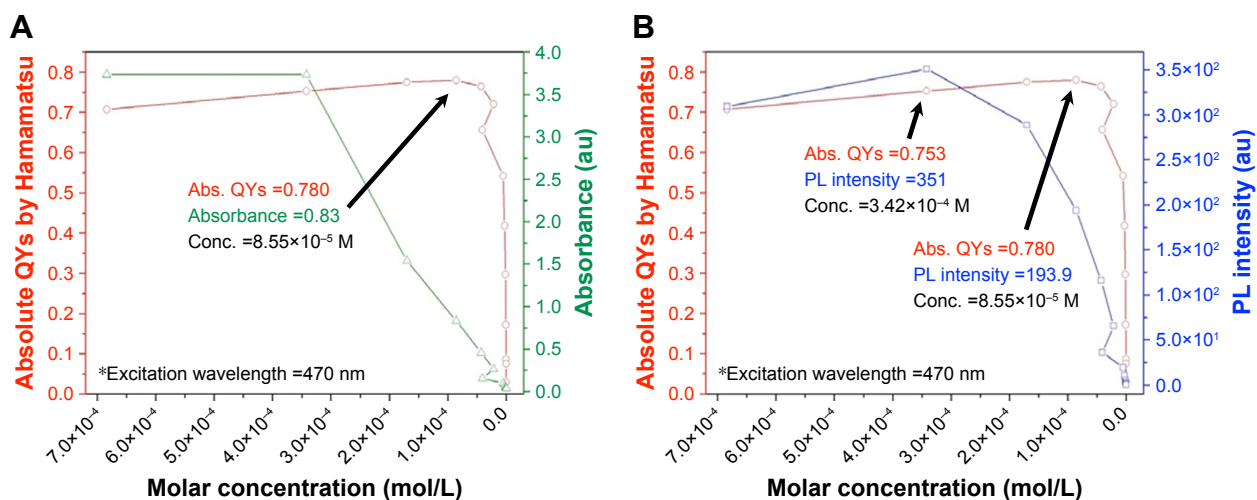
Supplementary materials

Figure S1 Absolute QYs of NI vs UV–visible absorption and vs PL emission at max in chloroform.
Notes: (**A**) Absolute QYs vs UV–visible absorption. (**B**) Absolute QYs vs PL emission at max. The optimal conditions for the dye are represented by the black arrows.
Abbreviations: PL, photoluminescent; QYs, quantum yields; Abs., absolute; Conc., concentration; max, maximum.
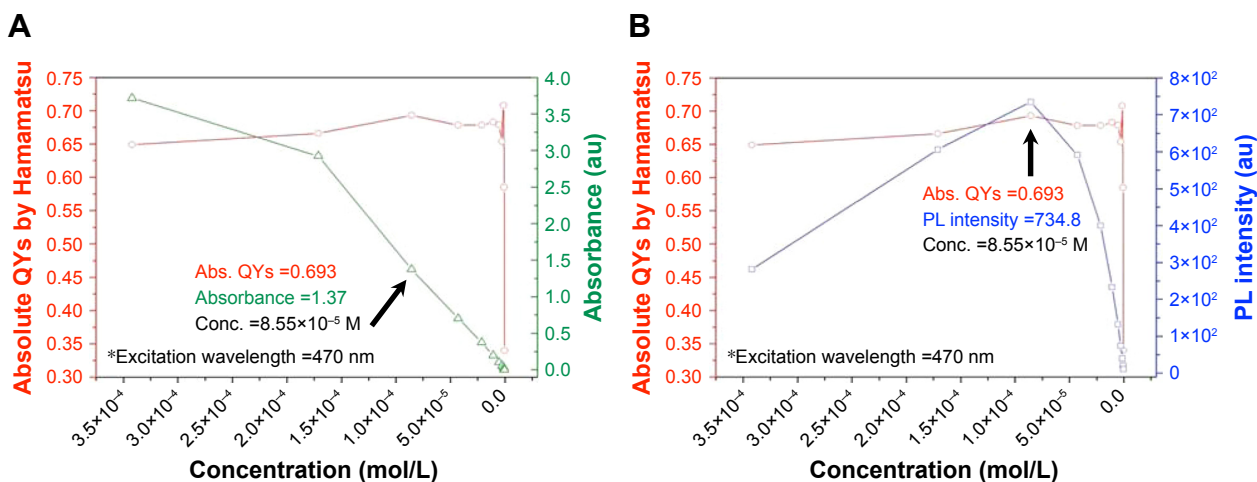

Figure S2 Absolute QYs of NI vs UV–visible absorption and PL emission at max in ethanol.
Notes: (**A**) Absolute QYs vs UV–visible absorption. (**B**) Absolute QYs vs PL emission at max. The optimal conditions for the dye are represented by the black arrows.
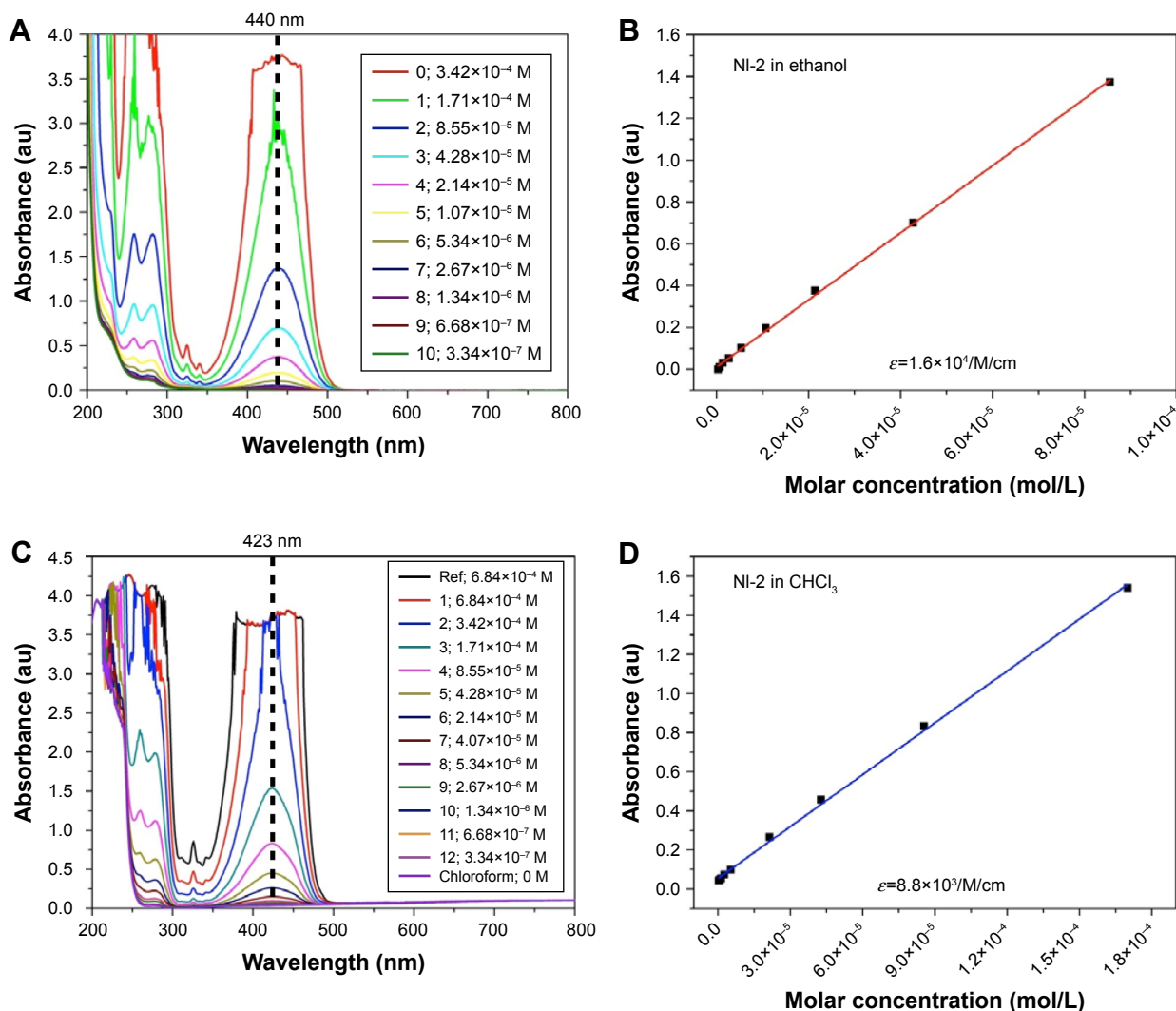**Abbreviations:** PL, photoluminescent; QYs, quantum yields; Abs., absolute; Conc., concentration; max, maximum.

Figure S3 Extinction coefficient of light absorbance of NI in chloroform and ethanol.

Notes: (**A**) UV-Visible spectra of NI-2 in ethanol; (**B**) standard curve and extinction coefficient (ε) of NI-2 in ethanol at 440 nm; (**C**) UV-Visible spectra of NI-2 in chloroform (CHCl3); (**D**) standard curve and extinction coefficient (ε) of NI-2 in ethanol at 423 nm.